ELEMENTA
Science of the Anthropocene

Influence of short-term synoptic events and snow depth on DMS, DMSP, and DMSO dynamics in Antarctic spring sea ice

Gauthier Carnat[1*] • Frédéric Brabant[1] • Isabelle Dumont[1] • Martin Vancoppenolle[2] • Stephen F. Ackley[3] • Chris Fritsen[4] • Bruno Delille[5] • Jean-Louis Tison[1]

[1]Laboratoire de Glaciologie, Faculté des Sciences, Université Libre de Bruxelles, Brussels, Belgium
[2]Laboratoire d'Océanographie et du Climat, CNRS, Paris, France
[3]University of Texas at San Antonio, One UTSA Circle, San Antonio, Texas
[4]Division or Earth and Ecosystem Sciences, Desert Research Institute, Reno, Nevada
[5]Unité d'Océanographie Chimique, MARE, Université de Liège, Liège, Belgium

*gauthier.carnat@gmail.com

Abstract

Temporal changes in the concentration profiles of dimethylsulfide (DMS), dimethylsulfoniopropionate (DMSP), and dimethylsulfoxide (DMSO) were measured in pack ice from the Bellingshausen Sea (Antarctica) during the winter-spring transition of 2007. Two sites with contrasting snow and ice thicknesses were sampled, with high concentrations of DMS, DMSP, and DMSO observed at both sites, especially in surface ice. These high concentrations were shown to correspond to the development of a surface ice microalgal community dominated by strong DMSP producers (flagellates and dinoflagellates) following flooding of the ice cover. Several short-term synoptic events were observed and shown to influence strongly the dynamics of sea ice DMS, DMSP, and DMSO. In particular, a cold spell event was associated with drastic changes in the environmental conditions for the sea ice microbial communities and to a remarkable increase in the production of dimethylated sulfur compounds at both sites. A good correlation between all dimethylated sulfur compounds, sea ice temperature, and brine salinity suggested that the observed increase was triggered mainly by increased thermal and osmotic stresses on microalgal cells. Atmospheric forcing, by controlling sea ice temperature and hence the connectivity and instability of the brine network, was also shown to constrain the transfer of dimethylated sulfur compounds in the ice towards the ocean via brine drainage. Analysis of the two contrasting sampling sites shed light on the key role played by the snow cover in the sea ice DMS cycle. Thicker snow cover, by insulating the underlying sea ice, reduced the amplitude of environmental changes associated with the cold spell, leading to a weaker physiological response and DMS, DMSP, and DMSO production. Thicker snow also hampered the development of steep gradients in sea ice temperature and brine salinity, thereby decreasing the potential for the release of dimethylated sulfur compounds to the ocean via brine drainage.

Domain Editor-in-Chief
Jody W. Deming,
University of Washington

Associate Editor
Jean-Éric Tremblay,
Université Laval

Knowledge Domain
Ocean Science

Article Type
Research Article

Part of an *Elementa* Special Feature
Biogeochemical Exchange Processes at Sea-Ice Interfaces (BEPSII)

Received: October 22, 2015
Accepted: September 20, 2016
Published: October 14, 2016

1. Introduction

The volatile organic compound dimethylsulfide (DMS) is the dominant biogenic sulfur compound in the ocean and the main contributor to the global biogenic sulfur flux to the atmosphere (Bates et al., 1992). Oceanic DMS is mainly produced by the enzymatic cleavage of the algal metabolite dimethylsulfoniopropionate (DMSP); its synthesis depends strongly on algal abundance, taxonomy, and various environmental stressors (Stefels et al., 2007). The physiological functions of DMSP in algal cells are not fully constrained. DMSP may act, for example, as an osmoregulator, a cryoprotectant, an antioxidant, or an overflow mechanism for excess energy dissipation (reviewed by Stefels et al., 2007). DMS is found supersaturated in all oceanic waters, leading to significant fluxes to the atmosphere where it is quickly oxidized in climate-active sulfate aerosol particles. These particles can potentially cool the climate by scattering and absorbing

solar radiation and promoting the formation of cloud condensation nuclei (Charlson et al., 1987). Although recent model simulations have strongly challenged the existence of a significant effect of DMS-derived aerosols at the global scale (Small et al., 2009; Quinn and Bates, 2011), DMS emissions are presumably relevant for the regional climate. Such relevance would be the case particularly in the clean atmosphere of remote polar regions, as suggested for instance by simultaneous observations of strong nucleation events and oceanic DMS pulses in the Arctic (Chang et al., 2011; Rempillo et al., 2011).

In polar regions, DMS emissions are strongly influenced by the presence of the seasonal ice cover which regulates gas exchange between the ocean and the atmosphere and seeds large phytoplankton blooms during seasonal melt. More than just a mechanical conduit, sea ice also represents a distinct biome favorable to substantial production of DMS (Tison et al., 2010; Nomura et al., 2011; Carnat et al., 2014; Damm et al., 2016). The significant biomass of sea ice microalgal assemblages (mean concentration of chlorophyll *a* [chl *a*] in Antarctic sea ice up to three orders of magnitude higher than the mean in the Southern Ocean; Arrigo et al., 2010) combined with the high levels of environmental stresses in their brine habitat support enhanced synthesis of metabolites such as DMSP (Kirst et al., 1991; Trevena et al., 2003). Hence, the contribution of sea ice assemblages to the polar sulfur cycle and regional climate must be considered. This need is particularly important in the recent context of a warming climate and changing sea ice cover.

Yet, this contribution remains very hard to assess. Direct measurements of sea ice–atmosphere DMS fluxes are technically challenging, and very few have been made so far (Zemmelink et al., 2008; Nomura et al., 2012). The poor spatio-temporal resolution of these measurements and the important heterogeneity of the sea ice environment further prevent regional extrapolations (Lana et al., 2011). Also, great gaps in our knowledge of DMS cycling in sea ice currently prevent accurate modeling of net DMS production by the sympagic biota. The net DMS production of a biome is a function of complex and rapid degradation and conversion processes between multiple methylated sulfur compounds (Stefels et al., 2007). For instance, DMS can be converted by bacterial and photochemical oxidation to a third dimethylated sulfur compound, dimethylsulfoxide (DMSO; Hatton et al., 2005). On the other hand, DMSO can also be reduced to DMS by bacteria or synthesized directly by algae, probably playing physiological functions similar to those of DMSP (Lee and de Mora, 1999). The dynamic of these processes and the relative importance of their different drivers (ecological and physico-chemical) in the specific environmental conditions of the brine habitat remain largely unknown. So far, only one study has provided estimates of the conversion rates of DMS, DMSP, and DMSO in natural brine samples (Asher et al., 2011).

Until now, sea ice DMS studies have essentially described the vertical and seasonal variability of DMS, DMSP, and DMSO concentrations (see Tison et al., 2010, and Carnat et al., 2014, for overviews). Several studies have also suggested links between this variability and sympagic algal abundance/taxonomy and environmental conditions (e.g., low temperature, high salinity, and oxidative stress) of the brine habitat (Kirst et al., 1991; Levasseur et al., 1994; Trevena and Jones, 2006; Damm et al., 2016). Regarding physical drivers, time-series studies have highlighted the influence of sea ice thermodynamics on the transport of dimethylated compounds towards the ocean. In summer, sea ice melting and the subsequent release of DMS and DMSP largely contribute to the DMS hot spots observed in the surface waters of marginal ice zones (Tison et al., 2010; Nomura et al., 2011). Significant amounts of dimethylated sulfur compounds could also be released to the under-ice water before melting through brine convection, provided the ice is permeable to fluid transport (Tison et al., 2010; Carnat et al., 2014; Galindo et al., 2014, 2015).

In this study, temporal changes in DMS, DMSP, and DMSO concentrations and a series of ancillary biogeochemical variables were obtained during the winter-spring transition of sea ice conditions in the Bellingshausen Sea, Antarctica. The observed changes are considered from the perspective of their connections with the thermal evolution of the sea ice cover. Sensitivity of the ice cover to atmospheric thermal forcing at short time intervals (days) in relation to its snow and ice thickness is also discussed.

2. Material and methods

2.1. Study area and sampling sites

The present study was conducted during the Sea Ice Mass Balance in Antarctica (SIMBA) experiment (Lewis et al., 2011) which took place onboard the RV/IB *Nathaniel B. Palmer* in the Bellingshausen Sea during September–October 2007. On arrival in the study area (Figure 1), the ship was moored to a large (~ 5 km^2) first-year drifting ice floe, named "Ice Station Belgica" (ISB; Figure 2), deemed large enough to survive the duration of the study. The floe was selected for its wide range of ice types and ice and snow cover thicknesses (Lewis et al., 2011) characteristic of the greater region. Two sites (named "Brussels" and "Liège") were chosen on the floe for sampling (Figure 2) based on three criteria: 1) homogeneity of the surface properties within each site (i.e., level ice and uniform snow thickness) to reduce within-site spatial variability; 2) great contrast in ice and snow properties between the chosen sites (Figure 3); and 3) sufficiently large area to conduct sampling in five independent but adjacent smaller zones at each site (Figure 2). The two sites were separated by ~ 1 km and located at a reasonable distance (0.8 and 1.8 km) from the

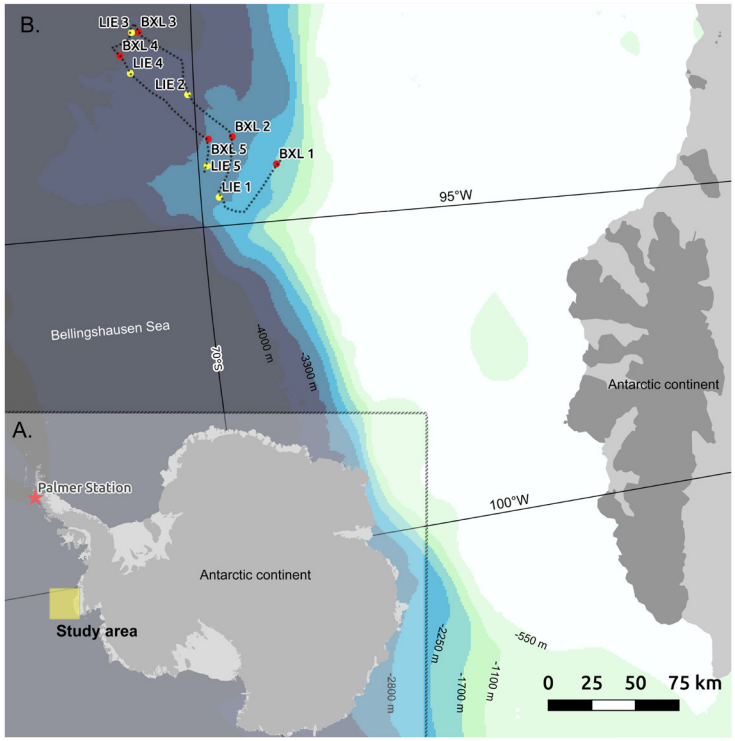

Figure 1

Location of the study area.

Location of the study area in the Bellingshausen Sea during the Sea Ice Mass Balance in Antarctica (SIMBA) experiment in 2007 (A). Location of the sampling events of the time series in the study area (B). Sampling events occurred at two sampling sites (named Brussels and Liège) located on a large first-year drifting ice floe named Ice Station Belgica (ISB). The dotted line represents the drift track of ISB during the study, as monitored by the ship anchored to the floe.

doi: 10.12952/journal.elementa.000135.f001

ship to minimize sample contamination. At each sampling site (Brussels and Liège), an undisturbed area of about 100 m x 60 m was delimited with flags. The two sites were sampled alternately every five days to build a time series. These sampling events were named Brussels 1–5 and Liège 1–5, respectively (Figures 2 and 3). Each time a site was sampled, a smaller square zone (10 m x 10 m) was delimited (Figure 2). These small zones were kept close to each other to minimize spatial variability and were kept undisturbed until their respective sampling day.

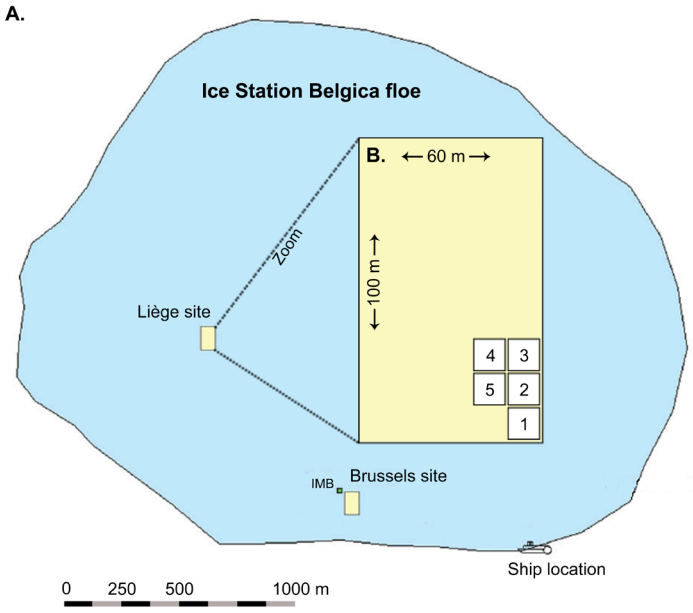

Figure 2

Layout of the drifting ice floe "Ice Station Belgica" (ISB).

Location of the sampling sites Brussels and Liège on ISB (A). IMB: Ice Mass Balance buoy. The zoomed area (B) shows the layout of each sampling site with the location chosen for each sampling event of the time series.

doi: 10.12952/journal.elementa.000135.f002

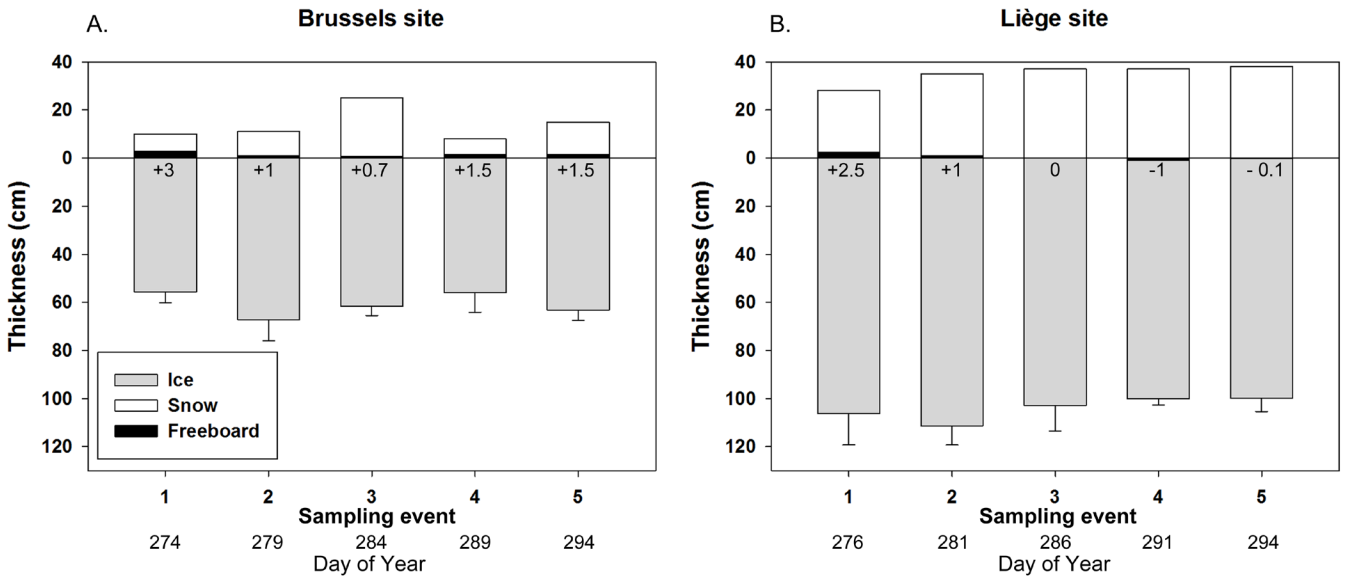

Figure 3

Time series of sea ice and snow thickness at the ISB sampling sites.

Freeboard values (distance between the snow/ice interface and the sea level) are indicated for each sampling event of the time series. A negative freeboard corresponds to a snow/ice interface submerged below sea level (flooding).

doi: 10.12952/journal.elementa.000135.f003

2.2. Atmospheric forcing and radiation data

Air temperature was recorded by an ice mass balance buoy (IMBB) deployed at the Brussels site (Figure 2; see Lewis et al., 2011, for details). Photosynthetically active radiation (PAR) and ultraviolet A (UV-A) and B (UV-B) data were acquired during the whole study by a GUV-2511 multi-channel radiometer (Biospherical Instruments Inc., San Diego, California) located on the ship deck (30.5 m above sea level; Vancoppenolle et al., 2011). The daily dose of PAR (400–700 nm) was computed as the time integral of instantaneous PAR readings. Spectral irradiance at selected wavelengths was used to reconstruct the spectral integral of UV-A and UV-B. Relationships to convert selected UV wavelengths to UV-A and UV-B irradiances were derived from a calibration radiometer deployed in the framework of the NSF UV monitoring Network operated by Biospherical Instruments Inc. at Palmer station (Figure 1) from April 2006 to July 2007. For UV-A (315–400 nm), a linear regression of the spectral irradiance at 380 nm was used ($R^2 = 0.997$; $p < 0.001$; $n = 20{,}667$) while for UV-B (290–315 nm), a multiple linear regression of spectral irradiance at 305 and 313 nm was used ($R^2 = 1$; $p < 0.001$; $n = 20{,}612$; Dr. G. Bernhard, Biospherical Instruments Inc., pers. comm., 2010). This reconstruction was made using the reasonable assumption that the difference between the radiation regime at Palmer station in the spring of 2006 and the radiation regime at the study area in the spring of 2007 was small. After conversion of instantaneous spectral irradiance readings into UV-A and UV-B irradiances, time integrals were computed to estimate the daily doses of UV-A and UV-B.

2.3. Sampling

For each sampling event, ice cores were taken using a 14 cm diameter electropolished stainless-steel (SS) corer. Ice cores were immediately wrapped in polyethylene bags and stored horizontally in an insulated box with cold packs (–30°C) to prevent brine drainage and limit the physiological activity of ice algae (Cox and Weeks, 1986; Stefels et al., 2012). Under-ice water was sampled at three depths (ice-ocean interface, 1 m, and 30 m) using a Masterflex E/S portable sampler (Cole Palmer®). The water was transferred into 20 ml glass vials which were immediately crimp sealed (butyl/PTFE septum cap), leaving no headspace. Vials were stored in the dark at 4°C.

2.4. Sea ice physical properties

Ice temperature and bulk ice salinity profiles were measured on the same dedicated ice core. Ice temperature was measured immediately after ice core extraction using a calibrated digital thermometer (Testo® 110) equipped with a fast response temperature probe (precision ± 0.2°C; Miller et al., 2015). The probe was inserted in holes drilled at the diameter of the probe perpendicularly to the ice core wall. The ice core was then cut with a vertical resolution of 5 cm and the sections were stored in sealed plastic containers. Bulk ice salinity was determined onboard on melted ice core sections using a calibrated Orion (Thermo Finnigan®) conductivity meter (precision ± 0.1; Miller et al., 2015). To assess the changes in permeability of the ice cover during the study, profiles of the relative brine volume fraction were computed assuming thermodynamic equilibrium of the brine with the surrounding ice (Cox and Weeks, 1983; Lepparänta and Manninen, 1988) and an assumed air volume fraction of 1%. Above a critical brine volume fraction, the interconnection

between brine inclusions becomes sufficient so that sea ice exhibits a sharp transition in its fluid properties (Golden et al., 1998; 2007). The critical value is highly dependent on the ice texture, being 5% for well-aligned columnar ice (Golden et al., 1998) and fluctuating between 7 and 10% for granular ice (Carnat et al., 2013; Zhou et al., 2013). Permeable ice is prone to brine convection provided the brine network is unstable; i.e., brine salinity (density) decreasing toward the ice-ocean interface and above the under-ice water salinity (density). Brine salinity was calculated from ice temperature according to Cox and Weeks (1983) and Lepparänta and Manninen (1988). Ice texture was described onboard from 2 mm thick sections of ice cores placed on a light table between crossed polarizers. The thick sections taken on the ice core were used later for determination of DMS, DMSP, and DMSO concentrations.

2.5. Algal biomass, taxonomy, and nutrients

Algal biomass was estimated from discrete chl *a* measurements performed on a dedicated ice core taken in close vicinity (few tens of cm) of the temperature-salinity and DMS, DMSP, DMSO ice cores. The ice core was cut onboard the ship with 10 cm vertical resolution. The samples were melted in a known volume of seawater (1:4 volume ratio), pre-filtered through 0.2 µm polycarbonate filters, and then filtered successively onto 10 µm and then 0.8 µm Nucleopore filters. This protocol is recommended to limit large temperature changes and osmotic stresses on microalgae (Miller et al., 2015). All filters were stored in cryovials at –80°C until analysis. Filters were extracted in acetone (90% volume ratio) in the dark at 4°C for 24 h, and chl *a* was quantified fluorometrically according to Yentsch and Menzel (1963). The total chl *a* content of the samples treated with the sequential filtration method was calculated as the sum of concentrations measured on the 10 µm and 0.8 µm filters. Under-ice water samples were filtered successively onto 10 µm and 0.8 µm Nucleopore filters before chl *a* measurement as described above.

The taxonomic composition of ice algal assemblages was determined in the home laboratory (Laboratoire de Glaciologie, Université Libre de Bruxelles, Belgium) on samples preserved in gluteraldehyde-Lugol solution (1% final concentration). Inverted light microscopy (100 and 320 x magnification) following Utermöhl (1958), and epifluorescence microscopy (400 x magnification) after DAPI staining (Porter and Feig, 1980), were used for this purpose. Autotrophic species were distinguished from heterotrophs by the red autofluorescence of chl *a* observed under blue light excitation. A minimum of 100 organisms was counted per taxonomic group. Microscopic size measurements were converted to cell volumes according to a set of geometric correspondences (Hillebrand et al., 1999). Autotrophic biomass was calculated from the abundance and the specific carbon biomass (carbon per cell) estimated from the relationships described in Menden-Deuer and Lessard (2000).

The inorganic nutrients NO_2^-, NO_3^-, NH_4^+, PO_4^{3-}, and $Si(OH)_4$ were determined at a 5 cm vertical resolution on a dedicated ice core. Ice core sections were melted in the dark at 4°C and then filtered through 0.4 µm polycarbonate filters. Nutrient concentrations were measured on filtrates following the protocol described by Papadimitriou et al. (2007). To avoid matrix effects, standards used for calibration were prepared in artificial seawater solutions with salinities similar to those of the analyzed samples. In order to better visualize the nutrient status of the ice cover, data were plotted as vertical profiles of the difference between the measured concentration of a nutrient and the concentration predicted by the theoretical dilution line (TDL).

2.6. DMS, DMSP, and DMSO concentrations

Sea ice cores and under-ice water samples were processed on the ship right after sampling to ensure the reliability of the DMS measurements. Analysis started systematically with the determination of DMS concentrations in under-ice water samples, which took less than 2 h. Then, DMS concentrations were determined on ice core sections stored at –30°C. This step typically took between 20 and 48 h, depending on the number of samples and replicates. This timing of analysis is considered as acceptable regarding the amount of DMS lost through diffusion during storage (Stefels et al., 2012; Carnat et al., 2014).

Sea ice cores were processed in a cold room (–30°C). Samples were cut from the central part of the ice core with 5 cm vertical resolution. DMS was extracted from samples using the method of dry crushing described in Stefels et al. (2012). In brief, the sample (~ 20 g) was placed with two SS marbles into an SS vessel specifically designed for the analysis of DMS in sea ice. The hermetically closed vessel was then fixed onto a crushing device and mechanically shaken (several hundred cycles min^{-1}) during four 45 s cycles in order to reduce the sample into a fine powder and ensure the release of all gas bubbles and brine inclusions from the ice matrix. After crushing, the vessel was connected to an extraction line and maintained at about –30°C during the purge of the vessel by UHP grade (99.999%) helium (He, 15 min at 50 ml min^{-1}). During this step, DMS is channeled out of the vessel and into a cryofocusing trap (PTFE loop immersed in liquid N_2, –196°C). DMS was then thermally desorbed by plunging the PTFE loop into boiling water and injecting it into a gas chromatograph (GC) for quantification. The procedure was repeated twice for each sample to ensure the recovery of all the DMS contained in the sample, as suggested by Stefels et al. (2012). The total DMS content of the sample was calculated as the sum of the two successive injections.

For the analysis of DMS in under-ice water samples, between 1 and 10 ml of liquid was subsampled from the 20 ml sampling vial and transferred through the septum into a clean pre-sealed 20 ml glass vial. The vial was then connected to a simple purge and trap system. The sampled was then purged with UHP grade He (30 min at 25 ml min^{-1}) and the DMS was trapped in a PTFE loop immersed in liquid N_2. DMS was then thermally desorbed by plunging the PTFE loop in boiling water and injected into a GC for quantification.

For the determination of total DMSP (particulate + dissolved fractions) in under-ice water samples, NaOH was added to the vial after the DMS analysis. This step brought the OH^- concentration above 2N and induced the hydroxide decomposition of DMSP in DMS and acrylic acid (Dacey and Blough, 1987). Vials were immediately crimp sealed (butyl/PTFE septum cap) and stored at 4°C in the dark for at least 24 h until analysis of DMSP as DMS following the procedure described above.

For DMSP and DMSO analysis in sea ice samples, the fine ice powder resulting from the crushing was recovered after the DMS quantification and divided into 20 ml glass vials. These were crimp sealed (butyl/PTFE septum cap) and stored at –30°C in the dark. For total DMSP, NaOH was added to the vials containing the ice powder. The vials were crimp sealed and stored to melt at 4°C in the dark until analysis as DMS. Total DMSO (particulate + dissolved fractions) was measured in the home laboratory a few months after sampling using the enzyme-linked method (Hatton et al., 1994) adapted for the determination of DMSO in sea ice as fully described by Brabant et al. (2011), with overall precision < 5%.

The gas chromatograph used for all quantifications was an Agilent 6890N equipped with a six-port switching valve, a Restek Rt-XLSulfur packed column (1 m x 0.75 mm internal diameter) and a flame photometric detector (FPD). The FPD was run either with a wavelength (394 nm) sulfur filter or with a wavelength (526 nm) phosphorus filter depending on the amount of DMS expected in the samples (based on the location of the DMS maxima observed during the first sampling events). The GC oven was operated using a temperature program (60–180°C) and calibrated against dilutions of pure (> 99%) DMS (Merck®) in ultra-pure water. The dilutions were performed at < 4°C to limit evaporation. The analytical precision of the method is < 10% for the quantification of DMS and DMSP.

2.7. Statistical analysis and figure drawing

The influence of the physical (temperature, bulk salinity, brine salinity, and brine volume fraction) and biological (algal biomass and nutrients) properties of the ISB ice cover on DMS, DMSP, and DMSO dynamics was investigated by computing non-parametric Spearman's rank-order correlation coefficients between variables (R, The project for Statistical Computing®). Spearman's rank-order coefficients were chosen instead of the usual Pearson's product-moment coefficients because of the heteroscedasticity of the data set. Pearson's product-moment coefficients require normally-distributed variables and the existence of a linear relationship between variables, whereas Spearman's rank-order coefficients only assess the strength of monotonic dependence between these variables. The relationship between variables was considered significant only when $p < 0.05$. Figures were drawn using SigmaPlot®11.0 and Adobe® Illustrator.

3. Results

3.1. Atmospheric forcing at ISB

Weather at ISB was typical of the Antarctic marine spring. Several recurring short-term synoptic events of variable intensity and length (4–8 days) were witnessed during the study. Cold and dry periods with generally clear-sky conditions associated with continental air masses from the South alternated with warm and wetter periods associated with oceanic air from the North (Vancoppenolle et al., 2011). As a result, important air temperature fluctuations were recorded during the study (Figure 4C). At least three alternating cycles of atmospheric cooling and warming were observed. Cooling cycles were typically the longest and most intense. Regarding radiation, PAR and UV-A daily doses (Figure 4A and 4B) increased with time at a mean rate of 62 µmol cm^{-2} d^{-1} ($R^2 = 0.734$; $p < 0.001$; $n = 24$) and 20 kJ m^{-2} d^{-1} ($R^2 = 0.80$; $p < 0.001$; $n = 24$), respectively. The UV-B doses showed more variability during the study period and no significant trend could be detected.

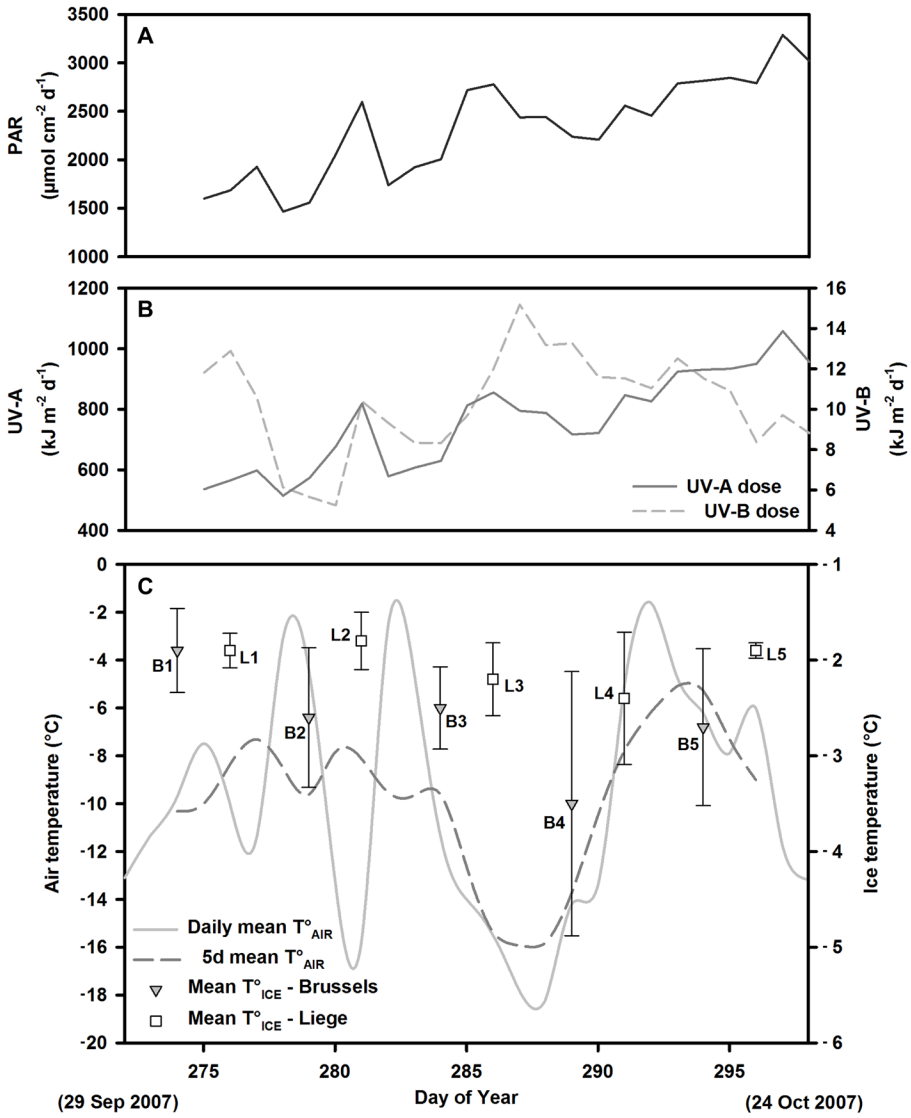

Figure 4

Time series of air temperature and solar radiation at ISB.

Time series of the photosynthetically active radiation (PAR) daily dose (A), UV-A (solid line) and UV-B (dashed line) daily doses (B), and air temperature in 1-day (solid line) and 5-day (dashed line) moving averages (C) recorded on the ship and by an ice mass balance buoy deployed at the Brussels site (Figure 2A). Also shown is the mean ice temperature (error bars indicate standard deviation; n = 11 – 22) recorded during the five sampling events at the Brussels (B1–B5, diamonds) and Liège (L1–L5, squares) sites.

doi: 10.12952/journal.elementa.000135.f004

3.2. Changes in sea ice and snow physical properties at ISB sampling sites

The Brussels and Liège sites displayed contrasting snow, ice thickness, and ice texture conditions (Figure 3). These conditions are presented in detail in Lewis et al. (2011). At the Brussels site, ice thickness ranged between 55 and 67 cm, while the snow cover ranged between 8 and 25 cm (Figure 3). The overall mean thickness of the ice was 60.9 cm ± 7.8 cm (n = 50). No decreasing trend (ANOVA) in ice thickness (indicative of bottom melting) was observed with time. The freeboard remained positive during each sampling event (0.7–3 cm) indicating that surface ice was not flooded during the study. The ice texture showed limited variation between sampling events and consisted mainly of columnar ice (see Lewis et al., 2011, for detailed ice stratigraphy of the ISB sampling sites). Snow ice was observed in surface ice layers.

At the Liège site, the ice and snow cover were significantly thicker (ANOVA, $p < 0.001$) than at the Brussels site, ranging between 99 and 106 cm and between 28 and 38 cm, respectively (Figure 3). The grand mean of the ice thickness was 104.3 cm ± 9.4 cm (n = 46). A linear decreasing trend with time (ANOVA, $p < 0.05$) was detected indicating bottom melting. The freeboard was negative at Liège 4 and 5, flooding the ice surface. The ice texture was more complex than at the Brussels site and was composed mainly of granular ice with inclusions of columnar ice and snow ice at different levels in the ice cover.

The Brussels and Liège sites also displayed contrasting thermohaline properties (Figure 5). At the Brussels site, the ice temperatures ranged between –1.5 and –6.1°C (Figure 5A). The main changes in temperature over time were observed in the top 40 cm of the ice cover, generally oscillating between cooling and warming events within a small temperature window (~ 1°C). A more dramatic shift in temperature was observed in the top 40 cm of Brussels 4 where the coldest temperature of the time series was recorded (–6.1°C). This minimum coincided with the most intense atmospheric cold spell recorded during the study

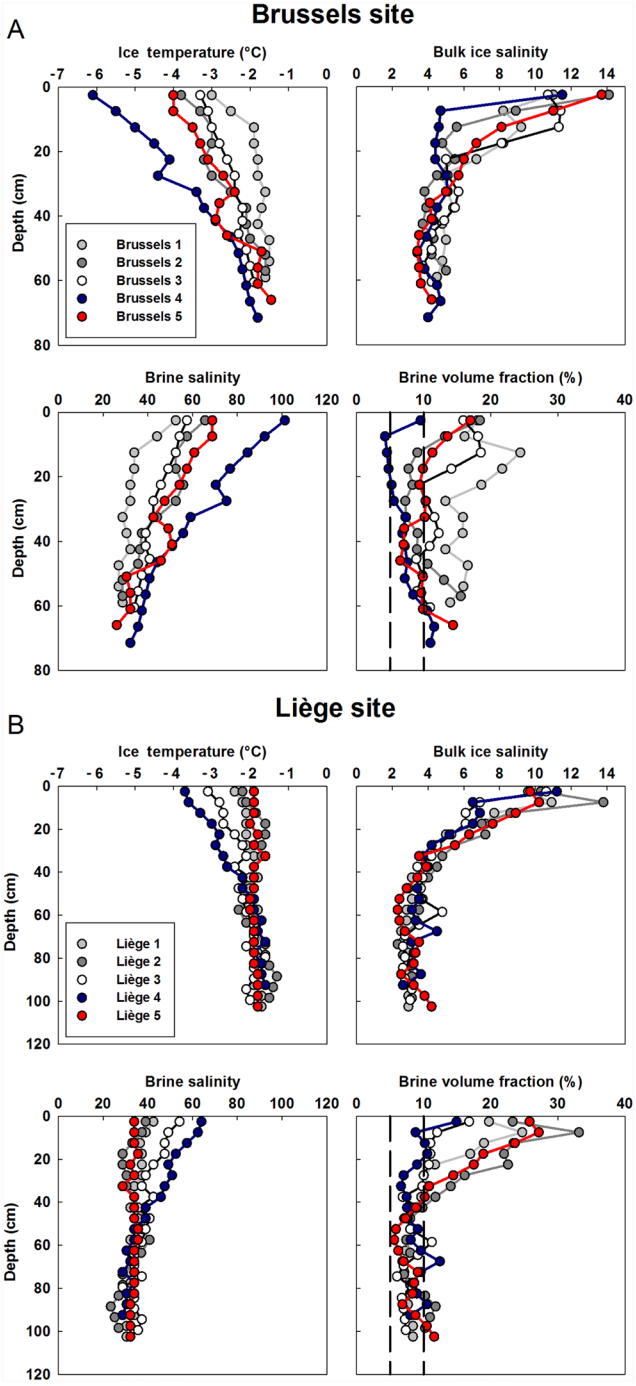

Figure 5

Time series of the thermohaline properties of the ice cover at the ISB sampling sites.

Comparative time series of ice temperature, bulk ice salinity, brine salinity, and relative brine volume fraction at the Brussels site (A) and Liège site (B). Note the difference in vertical scale between panel A and B. The 5 and 10% permeability thresholds are represented by vertical dashed lines on the brine volume fraction plots.

doi: 10.12952/journal.elementa.000135.f005

(Figure 4C). The bulk ice salinities ranged between 3.4 and 14.1. All profiles were C-shaped as usually observed in spring first-year sea ice (Eicken et al., 1991) but the C pattern was not symmetrically defined, as surface ice salinities were much higher than bottom ice salinities. The main changes were again observed in the top layers (30 cm). Interestingly, bulk ice salinities oscillated roughly in phase with the mean air temperature (higher values for Brussels 1, 3, and 5, and lower values for Brussels 2 and 4) suggesting cyclic net salt gain or loss in relation to the temperature regime. Brine volume fractions (Figure 5A) remained above 5% (permeability threshold for columnar ice) at all times and all depths except in the top 20 cm of the ice cover at Brussels 4. Brine salinity profiles (Figure 5A) underwent an apparent destabilization from Brussels 1 (values close to seawater salinity) to Brussels 4 where the highest values (up to 101) of the time series were observed in the top layers. Stability was restored at Brussels 5.

At the Liège site, changes in ice temperature, bulk ice salinity, and brine salinity observed between the different sampling events were smaller than those observed at the Brussels site under similar atmospheric

forcing (Figure 5B). The ice temperatures ranged between −1.3 and −3.7°C. The ice cover showed similar warm and isothermal temperature profiles at Liège 1, 2 and 5, with brine salinities close to seawater salinity. The ice cover cooled from Liège 3 to 4, when the coldest temperature and highest brine salinity of the time series were recorded, as also observed at the Brussels site. Substantial changes were strictly limited to the top 40 cm of the ice cover. The bulk ice salinities ranged between 2.3 and 13.8 (Figure 5B) and the mean salinity was systematically lower for the Liège cores than for the Brussels core. All profiles were C-shaped and showed little variation between sampling events. The oscillatory behavior of bulk ice salinity with mean air temperature was less obvious than at the Brussels site, with changes limited to the top 15 cm of less frequent occurrence. Brine volume fractions (Figure 5B) in the top 20 cm of the ice cover were at all times above 10% (the upper permeability threshold for granular ice). Values in the bottom two thirds of the cores were generally between 5 and 10%. Regarding temporal changes, the largest decrease was observed between Liège 2 and 4, similarly to the situation described for the Brussels site.

3.3. Changes in algal biomass, taxonomy, and nutrient concentrations at ISB sampling sites

The Brussels and Liège sites displayed contrasting biological properties (Figure 6, S1, S2). At the Brussels site, chl *a* ranged between 1.3 and 16 µg L^{-1} (mean = 5.9 µg L^{-1}). Maximum values were generally found in bottom ice, with secondary peaks in surface ice and low values in interior ice (Figure 6A). In bottom ice,

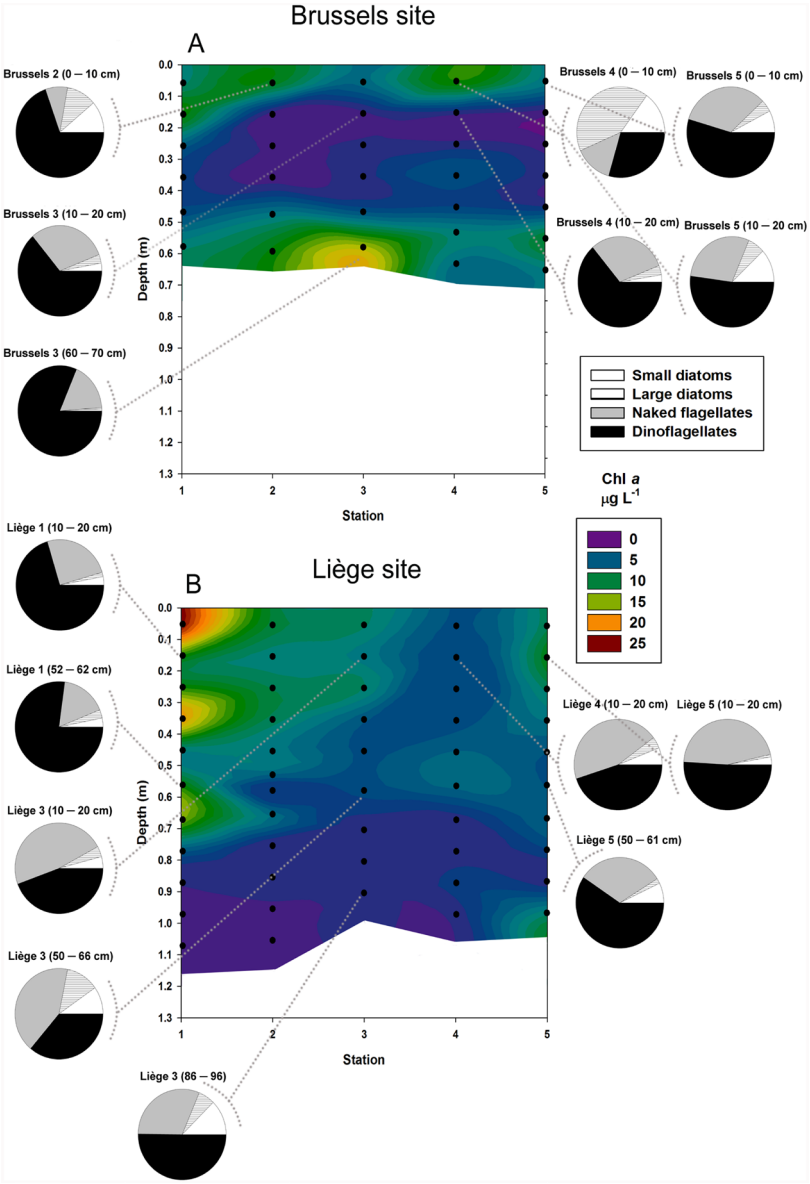

Figure 6

Time series of sea ice autotrophic biomass distribution and composition at the ISB sampling sites.

Comparative time series of chlorophyll *a* (chl *a*) concentration in sea ice at the Brussels site (A) and Liège site (B) using the color scale as indicated. Black dots indicate the mean sampling depths. Pie charts indicate the autotrophic biomass composition of the ice cover at selected sampling depths. The exact contribution of each microalgal group (in % and µg C L^{-1}) to the total biomass is provided in Table S1.

doi: 10.12952/journal.elementa.000135.f006

chl *a* increased gradually from Brussels 1 to 3 (maximum value of the time series), then sharply decreased towards the end of the study. Surface ice communities were essentially observed at Brussels 2 and 4. Regarding taxonomy, the ice cover was generally clearly dominated (in terms of biomass) by dinoflagellates, followed by naked flagellates, except for the surface ice at Brussels 4 where diatoms dominated (*Nitzschia longissimi* and *Plagiotropus sp.*; Figure 6A). A significant amount of empty diatom frustules was observed at Brussels 3. Nutrient concentration profiles (Figure S1) showed a strong depletion in NO_3^- during all sampling events, especially in the top layers. The Brussels ice cover was also generally slightly depleted in PO_4^{3-}, except for the ice-ocean interface (and the top layers at Brussels 1). On the other hand, a small enrichment in both NH_4^+ and NO_2^- was observed throughout the study. $Si(OH)_4$ showed the largest variations of all nutrients, with enriched values in the top half of the ice cover and depleted values in the bottom half (except at Brussels 1).

Chl *a* values measured at the Liège site (from 1.1 to 25.7 μg L^{-1}; mean = 6.6 μg L^{-1}) were comparable to those measured at the Brussels site, but the vertical distribution of the biomass and its temporal changes were drastically different (Figure 6B). Most of the biomass was observed at Liège 1, showing a vertical distribution characterized by an overall downward decrease with three local maxima. Ice layers below 60 cm depth generally exhibited low chl *a* values and showed, contrary to the Brussels site, no prevalence of a bottom ice community. Chl *a* drastically decreased from Liège 1 to 4, then slightly increased at Liège 5, especially in surface ice. Similarly to most samples of the Brussels site, Liège 1 communities were largely dominated by dinoflagellates. Subsequently, the contribution of dinoflagellates and naked flagellates became relatively equal (~ 40%) until the end of the study. A significant amount of *Phaeocystis sp.* was observed among the naked flagellates during all sampling events, and empty diatom frustules in interior ice at Liège 1, 3 and 5. Concentration profiles of NH_4^+, NO_3^-, and NO_2^- at the Liège site were generally comparable to those at the Brussels site, with a strong depletion in NO_3^- (especially in the top 20 cm layers) and a small enrichment in both NH_4^+ and NO_2^- (Figure S2). Concentrations of PO_4^{3-} were slightly below the TDL in the top half of the ice cover (except in the surface layers of Liège 5), and very close to the TDL in the bottom half. Similarly to the Brussels site, $Si(OH)_4$ is the nutrient that showed the largest variations in the ice, but this time with depleted values in surface (except at Liège 5) and interior ice, and enriched values near the ice-ocean interface.

Chl *a* concentrations in under-ice water (ice-ocean interface, 1 m, and 30 m depth) were low (data not shown) throughout the study period at the Brussels site (range = 0.01 to 0.19 μg L^{-1}; mean = 0.07 μg L^{-1}) as well as at the Liège site (range = 0.02 to 0.16 μg L^{-1}; mean = 0.08 μg L^{-1}).

3.4. Changes in DMS, DMSP, and DMSO concentrations at ISB sampling sites

As observed for the physical and biological properties of sea ice, the Brussels and Liège sites displayed contrasting profiles of DMS, DMSP, and DMSO concentrations (Figure 7). At the Brussels site, DMSP concentrations ranged from 75 to 5349 nM (mean = 899 nM; Figure 7A). DMS concentrations were generally lower, ranging from 6 to 2829 nM (mean = 300 nM; Figure 7B). DMSO was the dimethylated sulfur compound with the lowest concentrations in the ice, ranging from 5 to 775 nM (mean = 47 nM; Figure 7C). The three compounds globally showed similar vertical distribution and their temporal changes were highly synchronous. Highest values were always observed in the top 20 cm of the ice cover. Concentration profiles remained relatively stable between Brussels 1 and 2. A moderate increase in DMS, DMSP, and to a lesser extent DMSO occurred in the top half of the ice cover from Brussels 2 to 3. Then, a strong increase in all compounds was seen across the whole ice column from Brussels 3 to 4, when the maximum concentrations of the time series were recorded. From Brussels 4 to 5, concentrations decreased at all depths. During this sampling event, a bimodal (top and bottom 5 cm of the ice cover) distribution was observed for both DMS and DMSP, while no DMSO peak was detected at the ice-ocean interface.

At the Liège site, DMS, DMSP, and DMSO concentrations were generally lower than in the ice cover of the Brussels site (Figure 7). Also, all compounds varied within a narrower range, between 1.5 and 3352 nM for DMSP (mean = 253 nM; Figure 7D), between 0.6 and 1788 nM for DMS (mean = 121 nM; Figure 7E), and between 1.4 and 219 nM for DMSO (mean = 16 nM; Figure 7F). Similarly to the Brussels site, DMSO was the least abundant of the three compounds followed by DMS, and the highest DMS, DMSP, and DMSO values were always detected in the top 20 cm of the ice cover. Temporal changes in concentrations, on the other hand, differed slightly from those observed at the Brussels site. For instance, no major fluctuations between sampling events occurred below 30 cm depth for either of the compounds. Also, changes in the DMS, DMSP, and DMSO profiles were not as synchronous. In surface ice, concentrations of the three compounds increased between Liège 1 and Liège 2, then decreased towards Liège 3. An increase in DMS, DMSP, and DMSO was measured at Liège 4. However, contrary to Brussels 4, only DMSP showed its maximum value of the time series at this sampling event. Finally, as observed at Brussels 5, Liège 5 was characterized by a sharp decrease of DMS, DMSP, and DMSO.

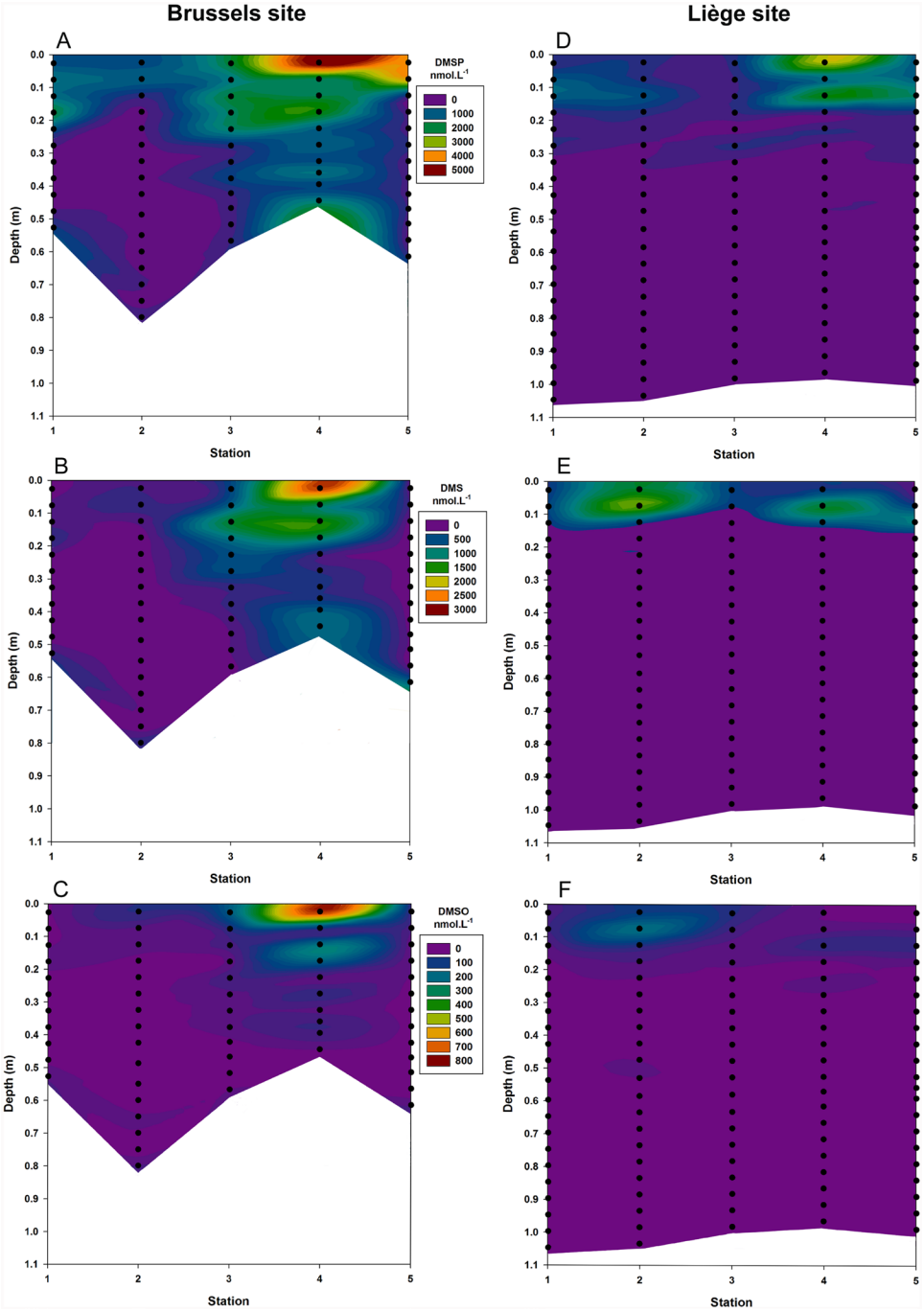

Figure 7

Time series of sea ice DMS, DMSP, and DMSO concentrations at the ISB sampling sites.

Comparative time series of DMSP (A and D), DMS (B and E), and DMSO (C and F) concentrations in sea ice at the Brussels (A–C) and Liège (D–F) sites using the color scales as indicated. Black dots indicate the mean sampling depths. Note the differences in color scales for the different sulfur compounds.

doi: 10.12952/journal.elementa.000135.f007

DMSP concentrations measured in under-ice water (ice-ocean interface, 1 m, and 30 m depth) at the Brussels site (ranging from 2 to 28 nM, mean = 14 ± 8 nM; Table 1) were significantly higher than typical spring open water values reported for the Southern Ocean (Lana et al., 2011). Highest levels were located in the uppermost meter of the water column. DMSP was found in the same order of magnitude at the Liège site (from 3 to 79 nM, mean = 18 ± 19 nM) but showed more variability close to the ice-ocean interface. At both sites, DMSP concentrations measured at 30 m depth were generally lower than at the interface and never exceeded 30 nM. DMS varied over a large range in the under-ice water at the Brussels site (from 1 to 126 nM, mean = 40 ± 33 nM) and was significantly higher than DMSP. The maximum value of the time series was measured at Brussels 2. Under-ice water DMS concentrations at the Liège site were in the range of those of DMSP (from 4 to 60 nM, mean = 23 ± 15 nM). The highest value was measured at Liège 3.

Table 1. Concentrations (nM) of DMS and DMSP measured at the ice-ocean interface and at 1-m and 30-m depth in the under-ice water of the Brussels and Liège sites

Compound measured	Depth under ice (m)	Brussels site					Liège site				
		Station 1	Station 2	Station 3	Station 4	Station 5	Station 1	Station 2	Station 3	Station 4	Station 5
DMS (nM)	0	ND[a]	49	43	54	38	15	4	41	36	8
	1	ND[a]	126	11	37	37	39	60	17	23	18
	30	ND[a]	1	ND[a]	36	9	18	20	21	15	6
DMSP (nM)	0	ND[a]	15	10	11	7	11	19	21	3	13
	1	ND[a]	25	19	18	15	6	15	79	20	23
	30	ND[a]	3	ND	28	2	4	4	38	10	3

[a]ND = no data

doi:10.12952/journal.elementa.000135.t001

4. Discussion

4.1. Importance of DMS, DMSP, and DMSO production at ISB

The concentrations of DMS and DMSP reported here are generally in the same order of magnitude as those reported in previous Antarctic sea ice studies and confirm that sea ice is a biome sustaining substantial production of dimethylated sulfur compounds. Concentrations measured at ISB were compared with the synthesis of Antarctic sea ice DMS and DMSP data sets provided in Carnat et al. (2014) and the recent works of Nomura et al. (2011) and Damm et al. (2016). The mean and maximum DMSP concentrations measured at the Brussels site were clearly the highest ever measured in level Antarctic first-year ice, and those measured at the Liège site were in the upper range of published values. These results indicate that the conditions prevailing at the time of sampling at ISB were particularly favorable for DMSP production. DMS data from sea ice are very scarce in the literature. DMS values are reported unfortunately as DMSP+DMS most of the time (e.g., Nomura et al., 2011) for methodological reasons (artificial conversion of DMSP to DMS when melting is used for extracting DMS from the ice matrix; see Stefels et al., 2012). The mean and maximum DMS concentrations measured at both sites were significantly higher than the values reported by Trevena and Jones (2006), Tison et al. (2010), and Carnat et al. (2014). DMSO data from Antarctic sea ice are even scarcer, with only one set of values obtained in the Weddell Sea during summer by Brabant et al. (2011; from 6 to 215 nM). Concentrations at the Brussels site largely exceeded those observed by Brabant et al. (2011), while those at the Liège site were within the same range. Interestingly, DMSO was a minor contributor to the total dimethylated sulfur pool in the two studies (2 to 7% in this study, 10–17% in Brabant et al., 2011), suggesting that this feature could be widespread in Antarctic sea ice. Such claim is supported by Asher et al. (2011) who recently identified DMSO reduction as a major pathway for DMS production in Antarctic sea ice.

The DMSP and DMSO bulk ice values reported here have not been compared to values from brine samples collected with the sackhole method in other studies (e.g., Asher et al., 2011), because the sackhole brine collection method (Gleitz et al., 1995) may lead to an underestimate of DMSP and DMSO concentrations when converted to bulk ice values. Indeed, the sackhole method fails to recover particulate matter efficiently (Brierley and Thomas, 2002). As a result, a substantial fraction of the DMSP pool, as shown by Tison et al. (2010), and potentially of the DMSO pool may be missed by this sampling approach.

The elevated under-ice water DMS and DMSP concentrations measured at ISB were generally consistent with observations made in under-ice water during brine drainage events in the spring (Carnat et al., 2014) and during the summer melting season (Trevena and Jones, 2006; Tison et al., 2010; Nomura et al., 2011). Values measured during some sampling events (Brussels 2 and 4, Liège 2 and 3) were among the highest ever reported in under-ice water samples, especially at 30 m depth.

4.2. Drivers of DMS, DMSP, DMSO production at ISB

4.2.1. Flooding events

Maximum DMS, DMSP, and DMSO concentrations at ISB were almost exclusively located in surface and sub-surface ice (Figure 7). This distribution contrasts sharply with the L-shaped DMS and DMSP profiles typically reported in Arctic sea ice studies (Levasseur, 2013; Galindo et al., 2014) and in some Antarctic sea ice studies (Tison et al., 2010; Nomura et al., 2011; Carnat et al., 2014). However, this distribution is comparable to DMSP profiles reported for flooded Antarctic sea ice (Trevena et al., 2000; Damm et al., 2016). The presence of snow ice in the Brussels 1 and Liège 1 ice cores indicates that flooding events certainly occurred at both sites prior to sampling. These events most likely set up the initial conditions of DMS, DMSP, and DMSO production observed in the ice cover at ISB. Seawater infiltration during flooding can bring microorganisms and nutrients in snow and surface ice, generally leading to the development of an important

surface microbial community (Tison et al., 2008; Saenz and Arrigo, 2012). These conditions can in turn lead to an increase in DMS, DMSP, and DMSO production in surface ice. As a result, the vertical distribution of concentrations differs radically from that of unflooded sea ice where bottom ice communities typically drive the dimethylated sulfur production (L-shaped profiles; e.g., Carnat et al., 2014). The similarity between the vertical distribution of chl *a* (Figure 6) and that of DMS, DMSP, and DMSO (Figure 7) at Brussels 1 and Liège 1, both showing surface maxima, supports the flooding scenario at ISB prior to sampling. The effect of flooding would have been more pronounced at the Liège site than at the Brussels site because of the thicker snowpack (Figure 3), which would explain the fact that chl *a* maxima were higher and extended deeper into the ice cover at Liège 1 than at Brussels 1 (Figure 7).

During the study itself, flooding events did not drastically modify DMS, DMSP, and DMSO production at ISB. The snowpack at the Brussels site was never thick enough to depress the surface of the ice below the freeboard layer. At the Liège site, flooding most certainly occurred at Liège 4 and 5, as indicated by the negative freeboard observed during these sampling events (Figure 3). This flooding may have replenished nutrients in the surface ice at Liège 5, as suggested by the increase in the concentrations of all nutrients in the top layers of the ice cover (Figure S2). It also likely affected the autotrophic biomass as shown by the general increase in chl *a* in the sub-surface layers (Figure 6B). However, these conditions were not associated with an increase in DMS, DMSP, and DMSO concentrations between Liège 4 and 5 (Figure 7D, E and F).

4.2.2. Algal biomass and taxonomy

The increase in surface ice algal biomass following flooding events likely determined the initial vertical distribution of dimethylated sulfur compounds in sea ice at ISB. Yet, algal biomass alone could not explain the very high DMS and DMSP production observed at ISB. Indeed, mean and maximum chl *a* measured at both the Brussels and Liège sites were in the lower range of values published in previous Antarctic sea ice DMS and DMSP studies (see the synthesis of Carnat et al., 2014). In fact, this finding was not surprising as the ability to produce DMSP is strongly species-specific (Stefels et al., 2007).

The presence of high DMSP-producing microalgal groups in the Brussels and Liège ice cover is a plausible explanation for the low chl *a*, high DMSP conditions that characterized both sampling sites. Indeed, the biomass at ISB was clearly dominated by flagellates and dinoflagellates (Figure 6), two groups known for their high intracellular DMSP quota (Stefels et al., 2007). In particular, cells of the flagellate *Phaeocystis sp.*, a very efficient DMSP producer, were observed during all sampling events at the Liège site. This situation contrasts strongly with other sea ice studies (Trevena and Jones, 2006; Tison et al., 2010; Carnat et al., 2014) where primary production was dominated by diatoms, known for their low intracellular DMSP quota (Stefels et al., 2007).

The predominance of flagellates and dinoflagellates at ISB was not surprising given the evidence for flooding events. Flagellates and dinoflagellates usually grow well in surface communities, while diatoms typically dominate in bottom ice communities (Thomas et al., 2010). For instance, dinoflagellates, by synthesizing elevated concentrations of mycosporine-like amino acids, are better adapted to the high UV radiations generally observed in the top layers of the ice, as reported by Fritsen et al. (2011) at ISB. Also, diatom growth can quickly become restricted by the nutrient shortage that characterizes surface ice in the absence of periodic refueling by flooding or brine convection. This restriction can lead to a shift in the dominant microalgal group from diatoms to flagellates and dinoflagellates. This scenario likely occurred at ISB prior to sampling. Flooding supplied nutrients to surface ice, as explained in section 4.2.1., favoring the initial development of diatoms in the ice cover. Because the ice cover was not refueled after the initial flooding events, NO_3^- became depleted and presumably curtailed diatom growth. This hypothesis was supported by the numerous empty frustules found in the ice cover at both sites and by the nutrient profiles (Figures S1 and S2) showing a strong depletion of NO_3^- throughout the study (especially in the top 20 cm of the ice). By contrast, low NO_3^- concentrations are expected to have a lesser effect on flagellates and dinoflagellates because these groups can more easily rely on other dissolved forms of N such as NH_4^+, as described in temperate seas by Tungaraza et al. (2003). As shown by the nutrient profiles, NH_4^+ was slightly enriched in surface ice at both sampling sites. The concept that differences in N-assimilation pathways within sea ice assemblages could play a role in determining the taxonomy of ice algal communities had already been proposed by Thomas et al. (2010).

Temporal changes in algal biomass and community composition over the duration of the study did not fully account for temporal changes in DMS, DMSP, and DMSO concentrations. Indeed, significant if weak correlations between chl *a* and DMS, DMSP, and DMSO were observed (Table 2), and the most important DMSP production event (Brussels 4) coincided with diatom-dominated assemblages (Figure 6A). Again, this finding was not surprising as DMSP synthesis is not only species-specific but also strongly dependent on the physiological conditions of the microalgal cells (Stefels et al., 2007). Strong positive correlations between chl *a* and DMSP have usually been reported during the spring-summer transition when primary production was largely dominated by bottom-ice diatom communities, such as in Trevena and Jones (2006), Tison et al. (2010), and Carnat et al. (2014). These communities typically develop in the relatively stable

Table 2. Spearman's rank-order correlation coefficients[a] for dimethylated sulfur compounds and other physical and biogeochemical variables in vertical profiles of ice at the Brussels and Liège sites

Variable	DMS	DMSO	DMSP
Brine salinity	0.43***	0.51***	0.54***
Temperature	–0.43***	–0.51***	–0.54***
Chlorophyll *a*	0.24**	0.22**	0.27***
NO_3^-	–0.57***	–0.64***	–0.72***
DMSP	0.86***	0.85***	–
DMSO	0.89***	–	–

[a]N = 149; significance level of $p < 0.01$ denoted by **; $p < 0.001$, by ***

doi:10.12952/journal.elementa.000135.t002

environmental/physiological conditions (e.g., temperature, salinity, nutrient availability) of the skeletal layer at the ice-ocean interface. Weaker relationships, on the other hand, were observed for other microalgal groups developing in surface and interior ice layers (e.g., Trevena et al., 2003; Damm et al., 2016). At the ISB sampling sites, primary production was clearly dominated by flagellates and dinoflagellates (Figure 6) thriving in the unstable environmental conditions of surface ice.

4.2.3. Environmental conditions

Robust correlations between ice temperature (negative) or brine salinity (positive) and either DMS, DMSP, and DMSO were observed during this study. Also, the most important DMS, DMSP, and DMSO production events at both sites (Brussels 4 and Liège 4; see Figure 7) were closely associated with the coldest surface ice temperatures and highest brine salinities of the time series (Figure 5). This association might suggest that the temporal variability in dimethylated sulfur compounds at ISB was at least partially driven by a physiological acclimation mechanism of microalgal cells to changes in the temperature and salinity of their ice habitat, with DMSP produced as osmoregulator and cryoprotectant (Kirst et al., 1991). It is generally assumed that, following thermodynamic equilibrium, the salinity of brine inclusions is solely determined by the ice temperature, with decreasing temperatures inducing increasing brine salinities (Petrich and Eicken, 2010). Survival of ice algae in brine inclusions therefore requires simultaneous protection against freezing and increased osmotic pressure of the medium. This environmental control of DMSP production is in good agreement with the work of Tison et al. (2010) which also reported a good correlation between DMSP and brine salinity, and with a few experiments showing the dependency of the DMSP intracellular quota on temperature (see Stefels et al., 2007, for an overview). It is also in good agreement with recent laboratory experiments conducted by Lyon et al. (2011, 2016). These authors subjected cultures of the sea ice diatom *Fragilariopsis cylindrus* to a progressive salinity shift in the lower range of sea ice brine salinities (from 35 to 70) and observed that intracellular DMSP increased by 85%.

Changes in ice temperature and brine salinity at the ISB sampling sites were mainly driven by short-term synoptic events, with the minimum ice temperature corresponding to the most intense atmospheric cold spell observed during the study (Figure 4C; see Lewis et al., 2011, for more details). Hence, the results presented here highlight the importance of atmospheric forcing in the sea ice DMS, DMSP, and DMSO cycle. In the same line of thinking, the overall lower DMS, DMSP, and DMSO concentrations measured at the Liège site (Figure 7) were likely the result of the insulation effect of the snowpack. Snow has a low thermal conductivity, about an order of magnitude lower than that of sea ice, and therefore acts as a thermal insulator, partially mitigating the effect of atmospheric cold spells on the underlying ice cover. The thicker snow cover at the Liège site provided better thermal insulation than the thin snow cover at the Brussels site (Figure 3), which resulted in higher ice temperatures (lower brine salinities) (Figure 5). This insulation in turn would have resulted in lower thermal and osmotic stresses on the ice algal cells, and hence in lower DMSP production.

Surface ice microalgal communities can also be exposed to important nutrient and radiative stresses. Regarding nutrients, the ice cover at both sites seemed NO_3^--depleted at all times (Figures S1 and S2). This limitation could have contributed to the high DMS and DMSP concentrations observed in the diatom-dominated community of the ice surface of Brussels 4 (Figures 6A, 7A, and 7B). Indeed, some diatom species can respond to N-limitation by increasing their DMSP intracellular quota (Sunda et al., 2007). DMSP would be produced to counteract the induced cellular oxidative stress on the one hand, and as an alternative to N-containing cellular osmolytes (saving N for other metabolic uses) on the other hand. Intracellular cleavage of DMSP into DMS and acrylate is very likely to ensue as those compounds are far more effective at scavenging hydroxyl radicals than DMSP (Sunda et al., 2002). Regarding radiative stresses, the increase in DMS and DMSP concentrations in the surface ice from Brussels 3 to 4, and Liège 3 to 4 also coincided with clear sky conditions, and hence high UV-B doses. High UV-B values have been shown to trigger dimethylated sulfur compounds production by microalgae following an antioxidant

cascade (Sunda et al., 2002). Again, this physiological response would be expected to be less pronounced at the Liège site because of the thicker snow cover.

4.2.4. Brine overturning events

The short-term synoptic events witnessed at ISB during the study (Figure 4C) also induced significant changes in the brine dynamics. These changes potentially influenced the vertical distribution of the dimethylated sulfur pools considerably, as well as the exchange of compounds at the ice-ocean interface. Cooling episodes were strong enough to allow unstable brine salinity (density) gradients to develop within the ice cover at both sites (Figure 5), especially at Brussels 4 and Liège 4. The development of such gradients can initiate the overturning of brine and its mixing with underlying seawater moving upward (brine drainage), provided the ice is permeable to fluid transport (Notz and Worster, 2009). Several physical observations strongly suggest that brine gravity drainage was a general feature at ISB, particularly at the Brussels site. For instance, excursions in the ice temperature profiles (McGuiness et al., 1998; Trodahl et al., 2001; Pringle et al., 2007) were reported by Lewis et al. (2011) in the IMBB measurements of the ISB floe. Also, Lewis et al. (2011) reported a marked difference between cooling and warming rates of the sea ice cover (i.e., clear faster warming of the entire ice cover at the end of the coldest air episode between Brussels 4 and 5), as expected in the case of brine overturning which enhances the heat transfer from the ocean to the ice. The oscillatory behavior of the bulk salinity profiles in the upper part of the ice also supported brine overturning (Figure 5A). Brine sinking will export salts from the surface layers, reducing the bulk ice salinity of these layers (e.g., Brussels 4). However, ascending warmer ocean water fueling the convection within the brine network will import new salts, stored in an increasing brine volume due to the combined effect of warmer brines and increasing air temperatures, increasing surface ice salinity (e.g., Brussels 5). Finally, specific features in the ice texture conditions also supported brine overturning. Ice dissolution features were seen on freshly extracted ice cores and on thick sections. Large vertical brine tubes, typical of brine drainage, initiating at the upper snow/congelation ice interface were observed and strongly contrasted with the typical tree-like structure of brine channels forming during the growth period. The tubes sometimes ran throughout the whole ice thickness and connected to the ice-ocean interface as inverted funnels, suggesting turbulent microflow developing as outgoing brines encounter warmer inflowing seawater.

Brine overturning events might have triggered a vertical redistribution of the dimethylated sulfur pools in the ice cover at the Brussels site. This possibility is supported by the increase in DMS, DMSP, and DMSO concentrations at all depths between Brussels 3 and 4, and the decrease of all compounds at all depths between Brussels 4 and 5. Similar redistributions by brine convection had already been suggested for DIC at the Brussels site (Geilfus et al., 2015), and for DMS and DMSP in other Antarctic sea ice studies (Tison et al., 2010; Carnat et al., 2014). Brine drainage might also have released substantial amounts of dimethylated sulfur compounds to the under-ice water. High DMS and DMSP concentrations were measured in under-ice water at both sites, showing an important variability between sampling events (Table 1). This observation, combined with the fact that chl *a* values in under-ice water remained very low at all times, suggests that the vast majority of DMS and DMSP found in the water column originated directly from the ice. Since bottom ice melting was relatively limited at the Liège site, and non-existent at the Brussels site, brine drainage is the best candidate to explain the transfer of compounds from the ice to the ocean. Such a process has previously been proposed for both Antarctic (Tison et al., 2010; Carnat et al., 2014) and Arctic (Galindo et al., 2014) sea ice. Interestingly, high DMS and DMSP concentrations were observed throughout the water column at both sites during sampling event 4, when conditions were the most favorable for brine drainage to occur. Whether these high concentrations at depth (30 m) were the result of sinking brine mixing with seawater or the result of another process (i.e., sinking of ice algal cells or fecal pellets) warrants future investigation.

Even if both the Brussels and Liège sampling sites were subjected to the same atmospheric forcing, the difference in ice texture and the thickness of snow and ice (Figure 3) likely resulted in weaker brine overturning events at the Liège site. The thicker snowpack and ice cover at the Liège site would have acted together to hamper the development of sharp temperature and brine salinity (density) gradients as observed at the Brussels site (Figure 5A). Furthermore, the thick layers of granular texture present in the Liège ice cover would have raised the brine percolation threshold. Recent field studies (Saenz and Arrigo, 2012; Carnat et al., 2013; Zhou et al., 2013) indeed suggest that columnar and granular ice exhibit different fluid transport properties, with the latter requiring higher brine volume fractions (between 7 and 10%) to become permeable to fluid flow than the threshold of 5% reported for columnar ice (Golden et al., 1998). Weaker brine overturning events at the Liège site would explain why the increase in DMS, DMSP, and DMSO concentrations from sampling event 3 to 4 remained restricted to the upper layer of the ice cover, while the increase at the Brussels site was observed at all depths (Figure 7). It would also explain the lower concentrations (and more moderate temporal variability) in under-ice water at the Liège site than at the Brussels site.

Brine overturning events could have also modified nutrient supply to sea ice microalgal communities, and hence their species composition and vertical distribution. Should brine overturning occur, a drastic

change in the concentration of nutrients in sea ice would be anticipated providing the draining brine and upward flowing seawater have different nutrient concentrations. Trends in the nutrient profiles (Figure S1, S2) support only one particular event of nutrient transport that could have been related to brine drainage: the disappearance of the local peak of PO_4^{3-}, $Si(OH)_4$, NH_4^+, and NO_2^- between Brussels 1 and 2. However, given the temporal sampling resolution adopted in this study, a rapid uptake rate of nutrients by sea ice algae or a rapid remineralization of organic matter by heterotrophs might have concealed or superseded the changes resulting from convective seawater exchange, as suggested in other studies (Riaux-Gobin et al., 2005; Fripiat et al., 2015).

4.3. Limitations and potential caveats of the study

The question might be asked whether the conditions and temporal changes observed at the Brussels and Liège sites were reliable and representative of the ISB floe. There is strong evidence in support of this case, at least for physical properties. The mean snow thickness measured at the ice core locations during the different sampling events are within the range of other snow thickness measurements performed elsewhere on the two sites (Lewis et al., 2011). Similarly, the mean ice thickness derived from the ice core length dataset at the Brussels site is consistent with the value of 0.591 ± 0.043 m reported by Lewis et al. (2011) from manual gauging and two IMBB time series measurements. The trend towards melting (–0.005 m d^{-1}) observed at the Liège site is also consistent with the IMBB records (–0.004 m d^{-1}) and with a computed mean value of ocean heat flux of 6 to 8 W m^{-2} during the study (Ackley et al., 2015).

The question might also be asked whether the results presented in this study were affected by spatial variability. Indeed, sea ice in the natural environment generally exhibits high spatial variability at different scales (Eicken et al., 1991). Both the sampling strategy followed during this study (see section 2.1) and the physical properties observed at the sampling sites suggest that spatial variability could be neglected with respect to the temporal variability in the interpretation of the differences between sampling events. Textural profiles revealed limited spatial variability between sampling square zones at the Brussels site, but a slightly higher heterogeneity at the Liège site (Lewis et al., 2011). Also, Lewis et al. (2011) showed a good similarity between comparative bulk salinity and $\delta^{18}O$ profiles measured at both sampling sites.

The overall lack of relationship between physical and biologically-mediated variables observed in this study is not surprising. In fact, such a lack of correlation is rather frequent in sea ice field studies and may be seen as the result of temporally decoupled physical and biological processes. The record of physical variables is to be considered as a snapshot, and the measurement of dissolved constituents as time-integrated information resulting from a suite of physical and biogeochemical processes (Meiners et al., 2009). This decoupling between variables is expected to widen further when an active brine drainage regime has settled within the ice cover, as in the course of this study. Also, this study focused on the influence of physical drivers on sea ice DMS, DMSP, and DMSO dynamics. The DMS biogeochemical cycle is characterized by many biologically-mediated conversion processes between DMS, DMSP, and DMSO (e.g., bacterial oxidation of DMS, bacterial reduction of DMSO, bacterial consumption of DMS and DMSP; Stefels et al., 2007). Such processes have been shown to occur at high rates in both the brine (Asher et al., 2011) and under-ice water medium (Galindo et al., 2015), and certainly affected the concentration profiles reported here to some extent. Microbial data (e.g., bacterial counts, gross or net production rates, degradation rates) are unfortunately not available. However, the strongly significant correlations between DMS, DMSP, or DMSO and physical and biogeochemical variables (Table 2) suggest that physical processes did indeed drive important temporal changes in all three of the dimethylated sulfur compounds. Nonetheless, in order to get a full picture of the sea ice DMS cycle, it would be very useful in future Antarctic sea ice studies to couple observations of the physical and thermodynamic state of the ice cover with measurements of microbial transformation rates.

5. Conclusions

This study provides insights into the cycling of DMS, DMSP, and DMSO in spring Antarctic sea ice. It specifically shows how the combined effect of snow accumulation and atmospheric cooling cycles can be conducive to elevated production of dimethylated sulfur compounds in surface ice. The additional overburden of thick snow results in seawater flooding of the ice surface. In turn, this flooding favors the development of surface microbial communities by supplying nutrient-rich seawater to the ice. Although this nutrient input appears to favor diatom growth initially, in the absence of further flooding events NO_3^- depletion returns and favors a shift in community composition towards groups (flagellates and dinoflagellates) known for their ability to synthesize high levels of intracellular DMSP. The DMSP production of these groups is potentially augmented by physiologically stressful environmental conditions (low temperatures, high salinities, high UV) in the surface ice habitat. Thermal, osmotic, and radiative stresses on surface communities can in turn be controlled by atmospheric forcing, with snow thickness modulating the amplitude of changes. Thickness of the snow pack and the cycling of atmospheric fronts also control the release of

dimethylated sulfur compounds to the under-ice water through brine drainage. Relatively thin ice cover (low insulation) and cold spell events favor low ice temperature (high brine salinity) in surface ice, and hence higher instabilities of the brine network.

Despite the episodic transfer of sulfur compounds to the ocean through brine drainage, DMS, DMSP, and DMSO dynamics in the ice cover at ISB resulted over the 20 day observation period in an overall net gain of 140 μmol of DMSP m^{-2}, and 14 μmol of DMS m^{-2} at the Brussels site, and of 104 μmol of DMSP m^{-2}, and 3 μmol of DMS m^{-2} at the Liège site (burdens calculated following Tison et al., 2010). The overall net gain of DMSO was substantially smaller, 5 μmol m^{-2} at the Brussels site, and close to 0 μmol m^{-2} at the Liège site. This pattern suggests that periodic forcing of the system by atmospheric thermal cycling maintains a sustained production of dimethylated sulfur compounds.

With the increasing occurrence of atmospheric anomalies in the Bellingshausen Sea comes an increased probability of witnessing wind-driven compaction of sea ice and greater precipitation (Stammerjohn et al., 2008) affecting the distribution of snow on the ice surface. Such changes may strengthen the impact of the physical and biogeochemical processes emphasized here and strongly modify DMS production and emissions at the regional scale.

References

Ackley SF, Xie H, Tichenor EA. 2015. Ocean heat flux under Antarctic sea ice in the Bellingshausen and Amundsen Seas: Two case studies. *Ann Glaciol* **56**(69). doi: 10.3189/2015AoG69A890.

Arrigo KR, Mock T, Lizotte MP. 2010. Primary producers and sea ice, in Thomas DN, Dieckmann GS, eds., *Sea Ice, Second Edition*. Oxford, UK: Wiley-Blackwell.

Asher EC, Dacey JWH, Mills MM, Arrigo KR, Tortell PD. 2011. High concentrations and turnover rates of DMS, DMSP, and DMSO in Antarctic sea ice. *Geophys Res Lett* **38**(L23609). doi: 10.1029/2011GL049712.

Bates TS, Lamb BK, Guenther A, Dignon J, Stoiber RE. 1992. Sulfur emissions to the atmosphere from natural sources. *J Atmos Chem* **14**: 315–337.

Brabant F, El Amri S, Tison JL. 2011. A robust approach for the determination of dimethylsulfoxide in sea ice. *Limnol Oceanogr-Meth* **9**: 261–274. doi: 10.4319/lom.2011.9.261.

Brierley AS, Thomas DN. 2002. Ecology of Southern Ocean pack ice. *Adv Mar Biol* **43**: 171–276. doi: 10.1016/S0065-2881(02)43005-2.

Carnat G, Papakyriakou T, Geilfus NX, Brabant F, Delille B, et al. 2013. Investigations on physical and textural properties of Arctic first-year sea ice in the Amundsen Gulf, Canada, November 2007-June 2008 (IPY-CFL system study). *J Glaciol* **59**(217): 819–837. doi: 10.3189/2013JoG12J148.

Carnat G, Zhou J, Papakyriakou T, Delille B, Goossens T, et al. 2014. Physical and biological controls on DMS,P dynamics in ice shelf-influenced fast ice during a winter-spring and a spring-summer transitions. *J Geophys Res: Oceans* **119**: 2882–2905. doi: 10.1002/2013JC009381.

Chang RYW, Sjostedt SJ, Pierce JR, Papakyriakou TN, Scaratt MG, et al. 2011. Relating atmospheric and oceanic DMS levels to particle nucleation events in the Canadian Arctic. *J Geophys Res-Atmos* **116** (D17). doi: 101.1029/2011JD015926.

Charlson RJ, Lovelock JE, Andreae MO, Warren SG. 1987. Oceanic phytoplankton, atmospheric sulphur, cloud albedo and climate. *Nature* **326**: 655–661.

Cox GFN, Weeks WF. 1983. Equations for determining the gas and brine volumes in sea-ice samples. *J Glaciol* **29**(102): 306–316.

Cox GFN, Weeks WF. 1986. Changes in the salinity and porosity of sea-ice samples during shipping and storage. *J Glaciol* **32**: 371–375.

Dacey JWH, Blough NV. 1987. Hydroxide decomposition of dimethylsulfoniopropionate to form dimethylsulfide. *Geophys Res Lett* **14**(12): 1246–1249. doi: 10.1029/GL014i012p01246.

Damm E, Nomura D, Martin A, Dieckmann GS, Meiners KM. 2016. DMSP and DMS cycling within Antarctic sea ice during the winter-spring transition. *Deep-Sea Res Pt II*. doi: 10.1016/j.dsr2.2015.12.015.

Eicken H, Lange MA, Dieckmann GS. 1991. Spatial variability of sea-ice properties in the northwestern Weddell Sea. *J Geophys Res: Oceans* **96**(C6): 10603–10615. doi: 10.1029/91JC00456.

Fripiat F, Sigman DM, Massé G, Tison JL. 2015. High turnover rates indicated by changes in the fixed N forms and their stable isotopes in Antarctic landfast sea ice. *J Geophys Res: Oceans* **120** (4). doi: 10.1002/2014JC010583.

Fritsen CH,Wirthlin ED, Momberg DK, Lewis MJ, Ackley SF. 2011. Bio-optical properties of Antarctic pack ice in the early austral spring. *Deep-Sea Res Pt II* **58**(9–10): 1052–1061. doi: 10.1016/j.dsr2.2010.10.028.

Galindo V, Levasseur M, Mundy CJ, Gosselin M, Tremblay JE, et al. 2014. Biological and physical processes influencing sea ice, under-ice algae, and dimethylsulfoniopropionate during spring in the Canadian Arctic Archipelago. *J Geophys Res-Oceans* **119**: 3746–3766. doi: 10.1002/2013JC009497.

Galindo V, Levasseur M, Scarratt M, Mundy CJ, Gosselin M, et al. 2015. Under-ice microbial dimethylsulfoniopropionate metabolism during the melt period in the Canadian Arctic Archipelago. *Mar Ecol-Progr Ser* **524**: 39–53. doi: 10.3354/meps11144.

Geilfus NX, Tison JL, Ackley SF, Galley RJ, Rysgaard S, et al. 2015. Sea ice pCO_2 dynamics and air-ice CO_2 fluxes during the Sea Ice Mass Balance in the Antarctic (SIMBA) experiment – Bellingshausen Sea, Antarctica. *The Cryosphere* **8**: 2395–2407. doi: 10.5194/tc-8-2395-2014.

Gleitz M, Rutgers van der Loeff M, Thomas DN, Dieckmann GS, Millero FJ. 1995. Comparison of summer and winter inorganic carbon, oxygen, and nutrient concentration in Antarctic sea ice brine. *Mar Chem* **51**: 81–91.

Golden KM, Ackley SF, Lytle VI. 1998. The percolation phase transition in sea ice. *Science* **282**: 2238–2241. doi: 10.1126/science.282.5397.2238.

Golden KM, Eicken H, Heaton AL, Miner J, Pringle DJ, et al. 2007. Thermal evolution of permeability and microstructure in sea ice. *Geophys Res Lett* **34**: L16501. doi: 10.1029/2007GL030447.

Hatton AD, Darroch L, Malin G. 2005. The role of dimethylsulphoxide in the marine biogeochemical cycle of dimethylsulphide. *Oceanogr Mar Biol* **42**: 29–56.

Hatton AD, Malin G, McEwan AG, Liss PS. 1994. Determination of dimethyl sulfoxide in aqueous solution by an enzyme-linked method. *Anal Chem* **66**(22): 4093–4096. doi: 10.1021/ac00094a036.

Hillebrand H, Dürselen CD, Kirschtel D, Zohary T, Pollingher U. 1999. Biovolume calculation for pelagic and benthic microalgae. *J Phycol* **35**: 403–424.

Kirst G, Thiel C, Wolff H, Nothnagel J, Wanzek M et al. 1991. Dimethylsulfoniopropionate (DMSP) in ice algae and its possible biological role. *Mar Chem* **35**(14): 381–388. doi: 10.1016/S0304-4203(09)90030-5.

Lana A, Bell TG, Simó R, Vallina SM, Ballabrera-Poy J, et al. 2011. An updated climatology of surface dimethlysulfide concentrations and emission fluxes in the global ocean. *Global Biogeochem Cy* **25**: GB1004. doi: 10.1029/2010GB003850.

Lee PA, de Mora SJ. 1999. Intracellular dimethylsulfoxide (DMSO) in unicellular marine algae: Speculations on its origin and possible biological role. *J Phycol* **35**: 8–18.

Lepparänta M, Manninen T. 1988. The brine and gas content of sea ice, with attention to low salinities and high temperatures. *Internal Report 88-2*. Helsinki: Finnish Institute of Marine Research.

Levasseur M. 2013. Impact of Arctic meltdown on the microbial cycling of sulphur. *Nat Geosci* **6**: 691–700. doi: 10.1038/ngeo1910.

Levasseur M, Gosselin M, Michaud S. 1994. A new source of dimethylsulfide (DMS) for the arctic atmosphere: ice diatoms. *Mar Biol* **121**: 381–387.

Lewis MJ, Tison JL, Weissling B, Delille B, Ackley SF, et al. 2011. Sea ice and snow cover characteristics during the winter-spring transition in the Bellingshausen Sea: An overview of SIMBA 2007. *Deep-Sea Res Pt II* **58**(9–10): 1019–1038. doi: 10.1016/j.dsr2.2010.10.027.

Lyon BR, Bennet-Mintz JM, Lee PA, Janech MG, DiTullio GR. 2016. Role of dimethylsulfoniopropionate as an osmoprotectant following gradual salinity shifts in the sea-ice diatom ***Fragilariopsis cylindrus***. *Environ Chem* **13**: 181–194. doi: 10.1071//EN14269.

Lyon BR, Lee PA, Bennett JM, DiTullio GR, Janech MG. 2011. Proteomic analysis of a sea-ice diatom: Salinity acclimation provides new insight into the dimethylsulfoniopropionate production pathway. *Plant Physiol* **157**(4): 1926–1941. doi: 10.1104/pp.111.185025.

McGuiness MJ, Trodahl HJ, Collins K, Haskell TG. 1998. Non-linear thermal transport and brine convection in first-year sea ice. *Ann Glaciol* **27**: 471–476.

Meiners KM, Papadimitriou S, Thomas DN, Norman L, Dieckmann GS. 2009. Biogeochemical conditions and ice algal photosynthetic parameters in Weddell Sea ice during early spring. *Polar Biol* **32**(7): 1055–1065. doi: 10.1007/s00300-009-0605-6.

Menden-Deuer S, Lessard EJ. 2000. Carbon to volume relationships for dinoflagellates, diatoms, and other protist plankton. *Limnol Oceanogr* **45**: 569–579.

Miller LA, Fripiat F, Else BGT, Bowman JS, Brown KA, et al. 2015. Methods for biogeochemical studies of sea ice: The state of the art, caveats, and recommendations. *Elem Sci Anth* **3**: 000038. doi: 10.12952/journal.elementa.000038.

Nomura D, Kasamatsu N, Tateyama K, Kudoh S, Fukuchi M. 2011. DMSP and DMS in coastal fast ice and under-ice water of Lützow-Holm Bay, eastern Antarctica. *Cont Shelf Res* **31**: 1377–1383. doi: 10.1016/j.csr.2011.05.017.

Nomura D, Koga S, Kasamatsu N, Shinagawa H, Simizu D. 2012. Direct measurements of DMS flux from Antarctic fast sea ice to the atmosphere by a chamber technique. *J Geophys Res* **117**: C04011. doi: 10.1029/2010JC006755.

Notz D, Worster MG. 2009. Desalination processes of sea ice revisited. *J Geophys Res* **114**: C05006. doi: 10.1029/2008JC004885.

Papadimitriou S, Thomas DN, Kennedy H, Haas C, Kuosa H, et al. 2007. Biogeochemical composition of natural sea ice brines from the Weddell Sea during early austral summer. *Limnol Oceanogr* **52**(5): 1809–1823. doi: 10.4319/lo.2007.52.5.1809.

Petrich C, Eicken H. 2010. Growth, structure and properties of sea ice, in Thomas DN, Dieckmann GS eds., *Sea ice, Second Edition*. Oxford, UK: Wiley-Blackwell.

Porter KG, Feig YS. 1980. The use of DAPI for identifying and counting aquatic microflora. *Limnol Oceanogr* **25**: 943–948.

Pringle DJ, Eicken H, Trodahl HJ, Backstrom LGE. 2007. Thermal conductivity of landfast Antarctic and Arctic sea ice. *J Geophys Res: Oceans* **112**(C4). doi: 10.1029/2006JC003641.

Quinn PK, Bates TS. 2011. The case against climate regulation via oceanic phytoplankton sulphur emissions. *Nature* **480**: 51–56.

Rempillo O, Seguin AM, Norman AL, Scarratt M, Michaud S, et al. 2011. Dimethyl sulfide air-sea fluxes and biogenic sulfur as a source of new aerosols in the Arctic fall. *J Geophys Res* **116**: D00S04. doi: 10.1029/2011JD016336.

Riaux-Gobin C, Tréguer P, Dieckmann G, Maria E, Vétion G, et al. 2005. Land-fast ice off Adélie Land (Antarctica): Short-term variations in nutrients and chlorophyll just before ice break up. *J Marine Syst* **55** (3–4): 235–248. doi: 10.1016/j.jmarsys.2004.08.003.

Saenz BT, Arrigo KR. 2012. Simulation of a sea ice ecosystem using a hybrid model for slush layer desalination. *J Geophys Res-Oceans* **117**(C5). doi: 10.1029/2011JC007544.

Small JD, Chuang PY, Feingold G, Jiang HL. 2009. Can aerosol decrease cloud lifetime? *Geophys Res Lett* **36**: L16806.

Stammerjohn SE, Martinson DG, Smith RC, Yuan X, Rind D. 2008. Trends in Antarctic annual sea ice retreat and advance and their relation to El Nino-Southern Oscillation and Southern Annular Mode variability. *J Geophys Res* **113**: C03S90. doi: 10.1029/2007JC004269.

Stefels J, Carnat G, Dacey JWH, Goossens T, Elzenga JTM, et al. 2012. The analysis of dimethylsulfide and dimethylsulfoniopropionate in sea ice: Dry-crushing and melting using stable isotope additions. *Mar Chem* **128–129**(20): 34–43. doi: 10.1016/j.marchem.2011.09.007.

Stefels J, Steinke M, Turner S, Malin G, Belviso S. 2007. Environmental constraints on the production and removal of the climatically active gas dimethylsulphide (DMS) and implications for ecosystem modelling. *Biogeochemistry* **83**: 245–275. doi: 10.1007/s10533-007-9091-5.

Sunda W, Hardison R, Kiene RP, Bucciarelli E, Harada H. 2007. The effect of nitrogen limitation on cellular DMSP and DMS release in marine phytoplankton: Climate feedback implications. *Aquat Sci* **69**(3): 341–351. doi: 10.1007/s00027-007-0887-0.

Sunda W, Kieber DJ, Kiene RP, Huntsman S. 2002. An antioxidant function for DMSP and DMS in marine algae. *Nature* **418**: 317–320. doi: 10.1038/nature00851.

Thomas DN, Papadimitriou T, Michel C. 2010. Biogeochemistry of sea ice, in Thomas DN, Dieckmann GS eds., *Sea Ice*, Second Edition. Oxford, UK: Wiley-Blackwell.

Tison JL, Brabant F, Dumont I, Stefels J. 2010. High-resolution dimethyl sulfide and dimethylsulfoniopropionate time series profiles in decaying summer first-year sea ice at Ice Station Polarstern, western Weddell Sea, Antarctica. *J Geophys Res* **115**: G04044. doi: 10.1029/2010JG001427.

Tison JL, Worby A, Delille B, Brabant F, Papadimitriou S, et al. 2008. Temporal evolution of decaying summer first-year sea ice in the Western Weddell Sea, Antarctica. *Deep-Sea Res Pt II* **55**: 975–987. doi: 10.1016/j.dsr2.2007.12.021.

Trevena AJ, Jones GB. 2006. Dimethylsulphide and dimethylsulfoniopropionate in Antarctic sea ice and their release during sea ice melting. *Mar Chem* **98**: 210–222. doi: 10.1016/j.marchem.2005.09.005.

Trevena AJ, Jones GB, Wright SW, van den Enden RL. 2000. Profiles of DMSP, algal pigments, nutrients and salinity in pack ice from eastern Antarctica. *J Sea Res* **43**: 265–273.

Trevena AJ, Jones GB, Wright SW, Van den Enden RL. 2003. Profiles of dimethylsulphoniopropionate (DMSP), algal pigments, nutrients and salinity in the fast ice of Prydz Bay, Antarctica. *J Geophys Res* **108**: (C5) 3145. doi: 10.1029/2002JC001369.

Trodahl HJ, Wilkinson SOF, McGuinness MJ, Haskell TJ. 2001. Thermal conductivity of sea ice: dependence on temperature and depth. *Geophys Res Lett* **28**(7): 1279–1282. doi: 10.1029/2000GL012088.

Tungaraza C, Rousseau V, Brion N, Lancelot C, Gichuki J, et al. 2003. Contrasting nitrogen uptake by diatom and ***Phaeocystis***-dominated phytoplankton assemblages in the North Sea. *J Exp Mar Biol Ecol* **292**: 19–41. doi: 10.1016/S0022-0981(03)00145-X.

Utermöhl H. 1958. Zur Vervelkommnung der quantitativen Phytoplankton-Methodik. *Mitt Int Verein Theor Angew Limnol* **9**: 1–38.

Vancoppenolle M, Timmermann R, Ackley SF, Fichefet T, Goosse H, et al. 2011. Assessment of radiation forcing data sets for large-scale sea ice models in the Southern Ocean. *Deep-Sea Res Pt II* **58**(9–10): 1237–1249. doi: 10.1016/j.dsr2.2010.10.039.

Yentsch CS, Menzel DW. 1963. A method for the determination of phytoplankton chlorophyll and phaeophytin by fluorescence. *Deep-Sea Res Oceanogr Abstr* **10**(3): 221–231. doi: 10.1016/0011-7471(63)90358-9.

Zemmelink HJ, Dacey JWH, Houghton L, Hintsa EJ, Liss PS. 2008. Dimethylsulfide emissions over the multi-year ice of the western Weddell Sea. *Geophys Res Lett* **35**: L06603. doi: 10.1029/2007GL031847.

Zhou J, Delille B, Eicken H, Vancoppenolle M, Brabant F, et al. 2013. Physical and biogeochemical properties in landfast sea ice (Barrow, Alaska): Insights on brine and gas dynamics across seasons. *J Geophys Res-Oceans* **118**(6): 3172–3189. doi: 10.1002/jgrc.20232.

Contributions

- Contributed to conception and design: GC, FB, SFA, BD, JLT
- Contributed to acquisition of data: GC, FB, ID, MV, SFA, CF, BD, JLT
- Contributed to analysis and interpretation of data: GC, FB
- Drafted and/or revised the article: GC, FB, JLT, BD
- Approved the submitted version for publication: GC, FB, MV, SFA, ID, CF, BD, JLT

Acknowledgments

The authors wish to thank the Captain and crew of the RV/IB *Nathaniel B. Palmer* and the science support team of Raytheon Polar Services. Sophie Berger is warmly thanked for her contribution to the mapping of the study area. This is a contribution to SCOR WG 140 on Biogeochemical Exchange Processes at Sea Ice Interfaces (BEPSII).

Funding information

G. Carnat benefited from a Belgian FRS-FNRS research grant (contract n° A 4/5 – MCF/DM – 2657). F. Brabant and I. Dumont benefited from a FRIA research grant with the Belgian FRS-FNRS. J.-L. Tison acknowledges the support of the Belgian Science Policy (contract n° SD/CA/03A) and of the Belgian FRS-FNRS (FRFC contract n° 2.4649.07). The SIMBA project was supported by the National Science Foundation under NSF Grant ANT 0703682 – Sea Ice Mass Balance in the Antarctic to UTSA and S.F. Ackley.

Competing interests

The authors have declared that no competing interests exist.

Data accessibility statement

Data will be accessible online via institutional repository following the permanent link: http://orbi.ulg.ac.be.

Supplemental material

- **Table S1. Contribution of four major algal groups to the total biomass (in % and µgC L^{-1}) of the ice cover at the Brussels and Liège sites. (Excel).**
  sDIA: small diatoms; lDIA: large diatoms; nFLA: naked flagellates; dFLA: dinoflagellates.
- **Figure S1. Time series of the nutrient status of the ice cover at the Brussels site. (TIFF).**
  Vertical profiles of the difference in concentration from the theoretical dilution line (TDL) of PO_4^{3-} (S1A), $Si(OH)_4$ (S1B), NH_4^+ (S1C), NO_2^- (S1D), and NO_3^- (S1E) at the Liège site. The solid lines with symbols show the difference

between the measured concentration and the concentration predicted by the mean TDL. Error bars represent the range of the difference considering the minimum and maximum slopes for the computation of the TDL. Note the difference in horizontal scales.

- **Figure S2. Time series of the nutrient status of the ice cover at the Liège site. (TIFF).**
  Vertical profiles of the difference in concentration from the theoretical dilution line (TDL) of PO_4^{3-} (S1A), $Si(OH)_4$ (S1B), NH_4^+ (S1C), NO_2^- (S1D), and NO_3^- (S1E) at the Liège site. The solid lines with symbols show the difference between the measured concentration and the concentration predicted by the mean TDL. Error bars represent the variation range of the difference considering the minimum and maximum slopes for the computation of the TDL. Note the difference in horizontal scales.